Nonuniform Electro-osmotic Flow on Charged Strips and Its Use in Particle Trapping

Shui-Jin Liu, Shyh-Hong Hwang, and Hsien-Hung Wei*

Department of Chemical Engineering, National Cheng Kung University, Tainan 701, Taiwan

Received July 10, 2008. Revised Manuscript Received September 8, 2008

In this article, we investigate theoretically electro-osmotic flow set up by charged strips on an otherwise uncharged surface. Starting with a single-strip problem we demonstrate that for simple polynomial surface charge distributions several basic solutions can be derived in closed forms constituted by the analogous idea-flow solutions, which provide a more lucid way of revealing the flow features. These solutions reveal two types of flow topology: simple draining-in/pumping-out streaming and a pair of microvortices for symmetric and antisymmetric surface charge distributions, respectively. For an arbitrary surface charge distribution, more complicated flow structures can be found by the superposition of these basic solutions. We further extend the analysis to two uniformly charged strips and show how the flow characteristics vary with the strips' dimensions and surface zeta potentials. The far-field velocity behavior is also asymptotically identified and indicates that the hydrodynamic nature of the flow is typically long-range. An application to particle trapping with electro-osmotic vortices is also investigated theoretically for the first time. We show that in collaboration with short-range attraction effects the trapping can be facilitated by symmetric vortices with a converging stagnation point, but not by asymmetric vortices.

I. Introduction

The recent advent of micro/nanotechnology has imparted renewed strategies in patterning or creating structures on small scales. This has also triggered growing demands in parallel processing and automation in an integrated, miniaturized device under the theme of "lab on a chip" or "total microanalysis system" (μTAS).[1] Because a device often involves a variety of operations, the ability to precisely control and manipulate underlying transport processes becomes the key to fulfilling specific functions of the device. Although much progress has been made toward this aim, electrokinetic actuation provides a promising means in microfluidic applications because not only can operations be carried out on an electrode-embedded portable platform without moving parts but also its unique transport features offer a diversity of manipulation capacities.[2−4]

The most common way to drive fluids using electrokinetic effects is through electro-osmotic flow (EOF), which arises from the movement of mobile charge clouds within thin electric double layers (10−100 nm) adjacent to a charged surface under the action of an applied field. Because most of the viscous dissipation occurs within the double layers, EOF in a macroscopic view acts like a slip flow with the characteristic Smoluchowski velocity[5]

$$U = -\frac{\varepsilon \zeta E_{\parallel}}{\eta} \tag{1}$$

where ε and η denote the permittivity and viscosity of the working electrolyte, respectively, ζ is the surface zeta potential across the double layer, and $E_{\parallel}$ is the applied field parallel to the surface. The minus sign here is attributed to the fact that it is the movement of the double-layer counterions that is responsible for the fluid motion.

Because eq 1 is independent of the macroscopic length scale, EOF in a microchannel virtually looks like a plug flow. Because this character can eliminate Taylor dispersion commonly encountered in pressure-driven flow, EOF is widely used in conveying analytes or the separation of charged species with electric fields.[6] Moreover, the flow resistance now goes like d^{-2} and hence becomes much smaller than pressure-driven flow whose resistance is proportional to d^{-4}, where d is the hydraulic radius. Also, because much higher electric fields can be rendered at small scales, EOF is more efficient at transporting samples in microdevices than conventional pressure forcing.

While EOF is advantageous in driving fluids on the microscale (despite possible joule heating or bubble problems), pure EOF (in the absence of pressure gradients) on uniformly charged surfaces, however, does not permit vortices or closed streamlines because of its irrotational flow nature. In addition, it often suffers mixing deficiencies or lacks the ability to manipulate the fluid motion. Pure EOF is also less desirable for trapping suspended particles or concentrate dilute samples because it cannot provide velocity gradients needed for these processes.

One remedy for these shortcomings is to create nonuniform EOF by patterning charge on surfaces. Because of the breakdown of the electrostatics−hydrodynamics similitude,[7] the fluid motion now becomes rotational and hence can render the nonzero vorticity needed to engineer the flow.[8,9] Nonuniform surface charge can occur on a number of occasions, for instance, due to surface defects[10] or the adsorption of foreign particles on surfaces.[11] It can also be caused by concentration/charge polarization induced by dc[12] or ac fields.[13] The phenomenon could be further mediated by Faradaic reactions[14] or electrothermal effects.[15,16] In all of

* Author to whom correspondence should be addressed. E-mail: hhwei@mail.ncku.edu.tw.

(1) Dittrich, P. S.; Tachikawa, K.; Manz, A. *Anal. Chem.* **2006**, *78*, 3887–3907.
(2) Morgan, H., Green, N. G. *AC Electrokinetics: Colloids and Nanoparticles*, Research Studies Press: Philadelphia, PA, 2003.
(3) Stone, H. A.; Stroock, A. D.; Ajdari, A. *Ann. Rev. Fluid Mech.* **2004**, *36*, 381–411.
(4) Squires, T. M.; Quake, S. R. *Rev. Mod. Phys.* **2005**, *77*, 997–1026.
(5) Probstein, R. F. *Physicochemical Hydrodynamics*; John Wiley & Sons: New York, 1994.
(6) Ghosal, S. *Electrophoresis* **2004**, *25*, 214–228.
(7) Ben, Y.; Chang, H. C. *J. Fluid Mech.* **2002**, *461*, 229–238.
(8) Brunet, E.; Ajdari, A. *Phys. Rev. E* **2006**, *73*, 056306.
(9) Qian, S.; Bau, H. H. *Anal. Chem.* **2002**, *74*, 3616–3625.
(10) Long, D.; Stone, H. A.; Ajdari, A. *J. Colloid Interface Sci.* **1999**, *212*, 338–349.
(11) Wang, S.; Hu, X.; Lee, L. J. *J. Am. Chem. Soc.* **2007**, *129*, 254–255.
(12) Dukhin, S. S.; Miller, R. *Colloid Polym. Sci.* **1991**, *269*, 923–928.

10.1021/la802183q CCC: $40.75
Published on Web 10/29/2008

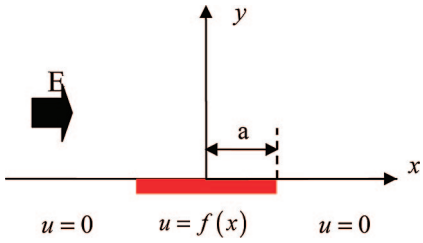

Figure 1. Two-dimensional EOF set up by a charged strip (highlighted in red) on an otherwise uncharged surface in a uniform electric field. The surface velocity on the strip is prescribed by the Smoluchowski formula with an arbitrary surface charge distribution.

these cases, the zeta potential of a surface is not constant and often varies with position. Because a practical microdevice often comprises different surfaces bearing distinct charges, the resulting EOF could exhibit a variety of features depending on the spatial variations of the surface zeta potentials and the interactions between local EOFs on different charged surfaces.

Motivated by the above, it is necessary to understand how an EOF behaves with various surface charge distributions or different arrangements of charged patterns. There have been a large number of studies on this subject, including analytical and numerical investigations on EOFs in various channel geometries with patterned surface charges or nonuniform zeta potential distributions[10,17−24] and their applications to solute transport processes.[25,26] While some physics and features have been revealed previously, we feel the need to seek a more detailed and fundamental understanding of nonuniformly charged EOF. In this work, we begin with the simplest scenario: an EOF set up by a charged strip on an otherwise uncharged surface in a dc electric field. As we will demonstrated in section II by expressing the surface charge distribution in a simple polynomial form, we can obtain an analytical solution for the flow field from which the underlying physics can be more directly revealed and identified. This approach also provides a systematic framework for solving a 2D EOF with an arbitrary charge distribution or pattern. In section III, we study the flow on two charged strips by constructing the solution via a superposition of those involved in single-strip problems, which enables us to decode complex flow interactions. An application using such a flow for particle trapping is illustrated in section IV. The article is concluded in section V.

II. EOF on a Single Charged Strip

II.A. Problem Formulation. Although practical EOFs occur in 3D microchannels, here we focus on a 2D EOF on a charged surface in an unbounded electrolyte solution. This approach enables us to elicit the genuine features of the flow without being complicated by the effects of proximate boundaries.

(13) Gonzalez, A.; Ramos, A.; Green, N. G.; Castellanos, A.; Morgan, H. *Phys. Rev. E* **2000**, *61*, 4019–4028.
(14) Lastochkin, D.; Zhou, R.; Wang, P.; Ben, Y.; Chang, H. C. *J. Appl. Phys.* **2004**, *96*, 1730–1733.
(15) Perch-Nielsen, I. R.; Green, N. G.; Wolff, A. *J. Phys. D: Appl. Phys.* **2004**, *37*, 2323–2330.
(16) Sigurdson, M.; Wang, D. Z.; Meinhart, C. D. *Lab Chip* **2005**, *5*, 1366–1373.
(17) Anderson, J. L.; Idol, W. K. *Chem. Eng. Commun.* **1985**, *38*, 93–106.
(18) Ajdari, A. *Phys. Rev. Lett.* **1995**, *75*, 755–758.
(19) Biddiss, E.; Erickson, D.; Li, D. *Anal. Chem.* **2004**, *76*, 3208–3213.
(20) Halpern, D.; Wei, H. H. *Langmuir* **2007**, *23*, 9505–9512.
(21) Qian, S.; Bau, H. H. *Appl. Math. Model.* **2005**, *29*, 726–753.
(22) Erickson, D.; Li, D. Q. *J. Phys. Chem. B* **2003**, *107*, 12212–12220.
(23) Ren, L. Q.; Li, D. Q. *J. Colloid Interface Sci.* **2001**, *243*, 255–261.
(24) Hlushkou, D.; Kandhai, D.; Tallarek, U. *Int. J. Numer. Methods Fluids* **2004**, *46*, 507–532.

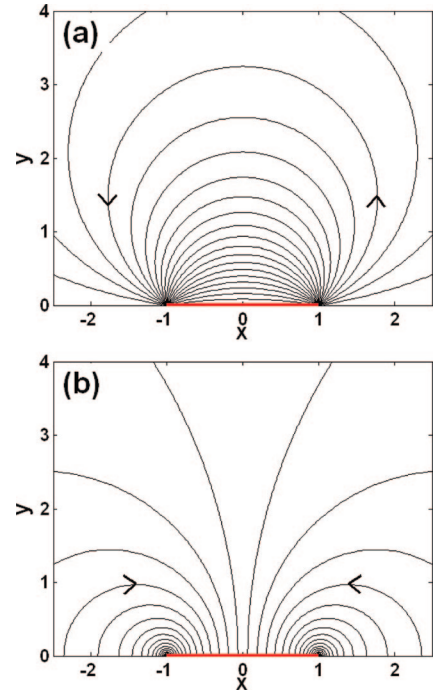

Figure 2. Streamlines of two ideal-flow solutions involved in our problem: (a) a point source and sink pair and (b) two oppositely rotating swirls.

The flow is driven by an electric field E parallel to the surface and is set up by a finite charged strip of width $2a$, outside of which there is no charge. See Figure 1. In the case in which the surface region outside the strip is uniformly charged, the effect is simply equivalent to that obtained by adding an EOF field created by a uniformly charged surface. Therefore, it suffices to examine the present problem. To nondimensionalize the problem, we scale lengths, fluid velocity, and pressure by a, $U_0 \equiv \varepsilon\zeta_0 E/\eta$, and $\eta U_0/a$, respectively, where ζ_0 is the amplitude of the zeta potential of the strip. Let p denote the pressure and $\mathbf{v} \equiv (u, v)$ denote the velocity field with u and v being respective velocity components in the horizontal (x) and vertical (y) directions. In the dimensionless form, the fluid motion is governed by the Stokes equations:

$$\nabla^2\mathbf{v} = \nabla p, \nabla\cdot\mathbf{v} = 0 \tag{2}$$

In the strip region ($-1 \le x \le 1$, $y = 0$), it is subjected to the Smoluchowski slip condition (eq 1) by assuming that the electric double layer is sufficiently thin compared to the strip dimension and there is vanishing normal velocity on the surface

$$u = f(x), v = 0 \tag{3a,b}$$

where $f(x)$ is the slip velocity distribution induced by a prescribed nonuniform surface charge or zeta potential distribution on the strip. For the rest of the surface, because it bears no charge, the no-slip condition is applied:

$$u = v = 0 \tag{4}$$

Far away from the surface, the velocity must vanish. That is,

$$\mathbf{v} \to 0 \text{ as } r = \sqrt{x^2 + y^2} \to \infty \tag{5}$$

A remark concerning the validity of our analysis is worth making below prior to solving the EOF problem above. Because a nonuniform surface charge distribution could cause bulk concentration gradients and induce a diffusio-osmotic flow (DOF), our analysis holds if the diffusio-osmostic velocity scale U_{DOF}

$= \{(\varepsilon/\eta)(kT/Ze)^2\}$ d ln C_s/dx is small compared to the Smoluchowski slip velocity given by eq 1, where kT is the thermal energy, Z is the valence of the supporting electrolyte, e is the elementary charge, and C_s is the electrolyte concentration at the outer edge of the double layer.[27] Because $C_s = 2C_0 \cosh(Ze\zeta/kT)$ from the Boltzmann distribution (with C_0 being the bulk concentration), we have $U_{DOF} \approx (\varepsilon/\eta)(kT/Ze)$ dζ/dx in terms of the zeta potential gradient. Hence, by comparing U_{DOF} with eq 1, diffusio-osmotic flow can be precluded if (kT/Ze)d ln ζ/d$x \ll E$; that is, the applied field must be sufficiently large compared to local zeta potential gradients.

To solve the flow problem with eqs 2−5, it is more convenient to adopt the stream function formulation. We define the stream function ψ in such a way that

$$u = \frac{\partial \psi}{\partial y} \text{ and } v = -\frac{\partial \psi}{\partial x} \tag{6}$$

which ensures that the continuity equation $\nabla \cdot \mathbf{v} = 0$ is satisfied automatically. Equation 2 then reduces to a biharmonic equation:

$$\nabla^2 \nabla^2 \psi = 0 \tag{7}$$

Applying boundary conditions (eqs 3−5) and taking Fourier transforms, we arrive at the solution for ψ:

$$\psi = \int_0^\infty [(A''(k) + A'(k)x + A(k)y)e^{-ky}] \cos(kx)\, dk + \int_0^\infty [(B''(k) + B'(k)x + B(k)y)e^{-ky}] \sin(kx)\, dk \tag{8}$$

The four coefficients A', A'', B', and B'' are identically zero because of zero normal velocity, and $\psi = 0$ on the surface in eq 4. Hence, the solution reduces to

$$\psi = y \int_0^\infty [A(k) \cos(kx) + B(k) \sin(kx)]e^{-ky}\, dk \tag{9}$$

with the coefficients

$$A(k) = \frac{1}{\pi}\int_{-1}^{1} f(x) \cos(kx)\, dx \text{ and}$$
$$B(k) = \frac{1}{\pi}\int_{-1}^{1} f(x) \sin(kx)\, dx \tag{10}$$

representing symmetric and antisymmetric parts of the solution, respectively.

II.B. Approach with Ideal-Flow Analogy and Its Implications. While the above mathematical layout provides a general formulation for solving the flow field on a single strip with an arbitrary surface charge distribution, we observe that the solution form (eq 9) is simply the product of y and an analogous ideal-flow solution. Here the analogous ideal-flow problem satisfies the Laplace equation with the same boundary conditions except that $f(x)$ in eq 10 is replaced by a stream function distribution on the strip. Two consequences immediately follow from this observation. First, because the flow now is no longer ideal, it must admit a vorticity that is set off by the velocity mismatch between the charged strip and the uncharged surface—the breakdown of the electrostatics−hydrodynamics similitude.

Second, mathematically speaking, the EOF solution here can be constructed simply by the analogous ideal-flow solution. As will be seen below, this ideal-flow solution consists only of simple source and sink solutions, which can be expressed explicitly in terms of spatial variables. This approach not only allows us to obtain the EOF solution in an explicit form, but also aids in our physical understanding by revealing quantitative features of the flow. Below, we first solve for the analogous ideal-flow problem. The EOF solution will then be given in the next subsection.

For the analogous ideal-flow problem, we find that all of the solutions are derived from the following two fundamental solutions

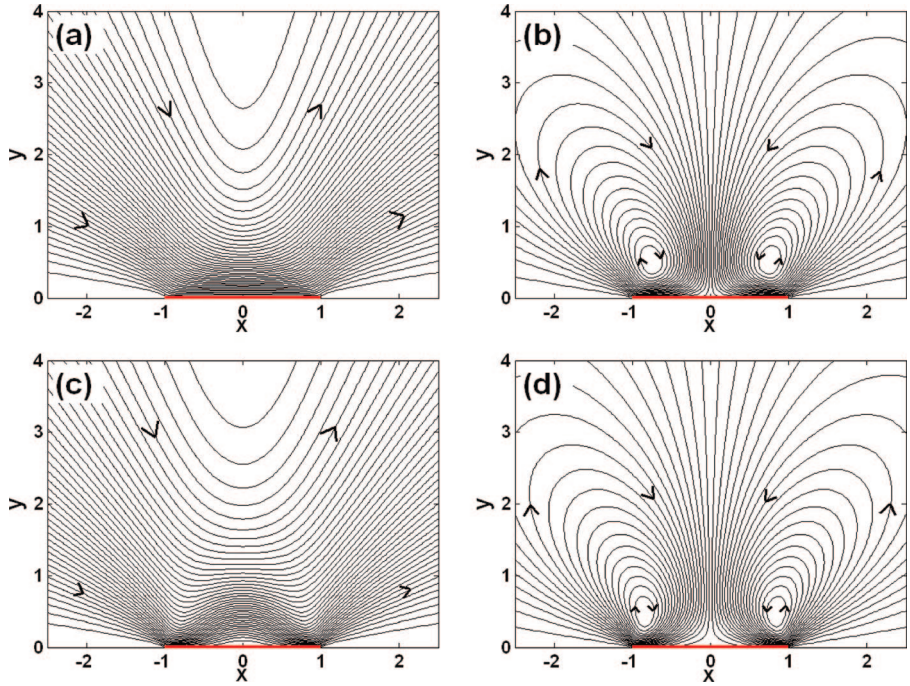

Figure 3. Streamlines of EOF with surface charge distributions: (a) $f = 1$ (b) $f = x$ (c) $f = x^2$, and (d) $f = x^3$. The electric field is toward the right. For symmetric charge distributions (a, c), the flow shows a simple draining-in/pumping-out streaming, whereas for asymmetric distributions (b, d), the flow exhibits a pair of microvortices.

$$\chi_1 = \frac{1}{\pi}\tan^{-1}\left(\frac{2y}{x^2+y^2-1}\right),$$
$$u_1 = \frac{1}{\pi}\left[\frac{2(x^2-y^2-1)}{(x^2+y^2-1)^2+4y^2}\right],$$
$$v_1 = \frac{1}{\pi}\left[\frac{4xy}{(x^2+y^2-1)^2+4y^2}\right] \quad (11a)$$

$$\chi_2 = \frac{1}{2\pi}\ln\left[\frac{(x+1)^2+y^2}{(x-1)^2+y^2}\right],$$
$$u_2 = \frac{1}{\pi}\left[\frac{-4xy}{(x^2+y^2-1)^2+4y^2}\right],$$
$$v_2 = \frac{1}{\pi}\left[\frac{2(x^2-y^2-1)}{(x^2+y^2-1)^2+4y^2}\right] \quad (11b)$$

where χ_1 and χ_2 are stream functions with the corresponding velocity fields (u_1, v_1) and (u_2, v_2). As illustrated in Figure 2, by rewriting these ideal-flow solutions in twin polar coordinates with origins at the outer edges of the strip, it can be easily recognized that eq 11a represents a radial source and sink pair located at the two edges of the strip and that eq 11b is a similar solution consisting of two oppositely rotating swirls. Because these ideal-flow solutions are essentially made by a point source and sink pair, the corresponding far-field ($r = \sqrt{(x^2+y^2)} \to \infty$) behaviors look like dipoles whose velocities decay at a rate of $1/r^2$, as shown in Appendix I.

II.C. Flow Fields and Their Characteristics. Now we solve for the EOF problem. Similar to simple harmonic expansions for solving ideal-flow problems,[28] we write the prescribed surface charge distribution in the polynomial form:

$$f(x) = \sum c_n x^n \quad (12)$$

Here we retain only the terms up to the cubic term, which suffices to describe most of the surface charge distributions in practice. For each distribution, we determine the corresponding stream function and velocity field. After taking inverse Fourier transforms, we find that all of the solutions can be constituted by the two ideal-flow solutions given by eqs 11a and 11b. As a result, these EOF solutions can be derived in closed forms below and written explicitly in terms of spatial variables.

(i) For uniform $f = 1$

$$\psi = y\chi_1, u = \chi_1 + yu_1, v = yv_1 \quad (13)$$

(ii) For linear $f = x$,

$$\psi = yx\chi_1 - y^2\chi_2,$$
$$u = x\chi_1 + yxu_1 - 2y\chi_2 - y^2u_2,$$
$$v = -y\chi_1 + yxv_1 + y^2v_2 \quad (14)$$

(iii) For quadratic $f = x^2$,

$$\psi = (x^2y - y^3)\chi_1 - 2xy^2\chi_2 + \frac{2}{\pi}y^2,$$
$$u = (x^2 - 3y^2)\chi_1 + (x^2y - y^3)u_1 - 4xy\chi_2 - 2xy^2u_2 + \frac{4}{\pi}y,$$
$$v = -2xy\chi_1 + (x^2y - y^3)v_1 + 2y^2\chi_2 - 2xy^2v_2 \quad (15)$$

(iv) For cubic $f = x^3$,

$$\psi = (x^3y - 3xy^3)\chi_1 + (y^4 - 3x^2y^2)\chi_2 + \frac{4}{\pi}xy^2,$$
$$u = (x^3 - 9xy^2)\chi_1 + (x^3y - 3xy^3)u_1 + (4y^3 - 6x^2y)\chi_2 + (y^4 - 3x^2y^2)u_2 + \frac{8}{\pi}xy,$$
$$v = 3(y^3 - x^2y)\chi_1 + (x^3y - 3xy^3)v_1 + 6xy^2\chi_2 + (y^4 - 3x^2y^2)v_2 - \frac{4}{\pi}y^2 \quad (16)$$

The corresponding far-field behaviors for the above solutions are provided in Appendix II. In fact, we find that for a charge distribution with an arbitrary integer power in x, the solution can be written in a complex-variable form, which is given in Appendix III.

Figure 3a−d shows the streamlines for the surface charge distributions listed above. For symmetric charge distributions (i) and (iii), Figure 3a,c shows that the fluid is sucked toward the strip at one end and then ejected toward the bulk at the other, as if a moving object pushed (dragged) the fluid ahead (behind). Because the effect creates pumping with a constant flow rate, the velocity field must decay at a rate of $1/r$ to maintain mass conservation of fluid flow over a control volume of an arbitrarily large size r, which is consistent with the large-r behaviors in eqs 13 and 15 (cf. eqs A3 and A5 in Appendix II). Alternatively, the flow resembles the motion of a free falling object in an otherwise quiescent fluid so that the far-field flow behavior must behave like that induced by a point force (i.e., Stokeslet) at the same attenuation rate.

As for antisymmetric charge distributions (ii) and (iv), because the surface velocity on one half of the strip is identical to that on the other half but in the opposite direction, the opposition between these velocities results in a pair of symmetric vortices, as shown in Figure 3b,d. Also, because there is no net flow rate here, the far-field velocity must decay at a rate of $1/r^2$ or faster, consistent with those in eqs 14 and 16 (cf. eqs A4 and A6 in Appendix II).

Having the EOF solutions (eqs 13−16) ready for various surface charge distributions, we can construct a flow solution with an arbitrary surface charge distribution simply by a superposition of these solutions. Figure 4 is an example and shows a draining-in/pumping-out stream pattern with a small recirculating eddy, a combination of the flow features of both symmetric and antisymmetric cases.

II.D. Extension to EOF in Nonuniform Applied Fields. Given the fact that the surface velocity distribution $f(x)$ actually lumps the contributions from the surface charge (via the zeta

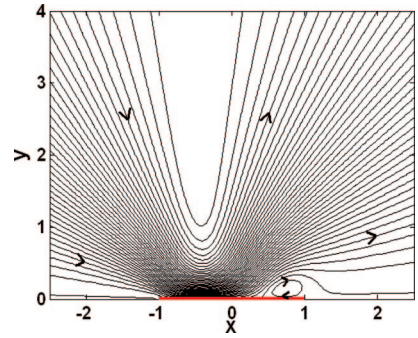

Figure 4. Streamlines with asymmetric surface charge distribution $f = x^3 - 0.4x^2 - x + 0.4$. The flow exhibits a draining-in/pumping-out streaming with a small recirculating eddy.

(25) Ghosal, S.; Lu, Z. Technical Proceedings of the 2002 International Conference on Simulation of Microsystems; *Nano Science and Technology Institute:* San Juan, Puerto Rico, 2002.
(26) Gleeson, J. P. *J. Colloid Interface Sci.* **2002**, *249*, 217–226.
(27) Anderson, J. L. *Ann. Rev. Fluid Mech.* **1989**, *21*, 61–99.
(28) Milne-Thomson, L. M. *Theoretical Hydrodynamics*; Macmillan: London, 1968.

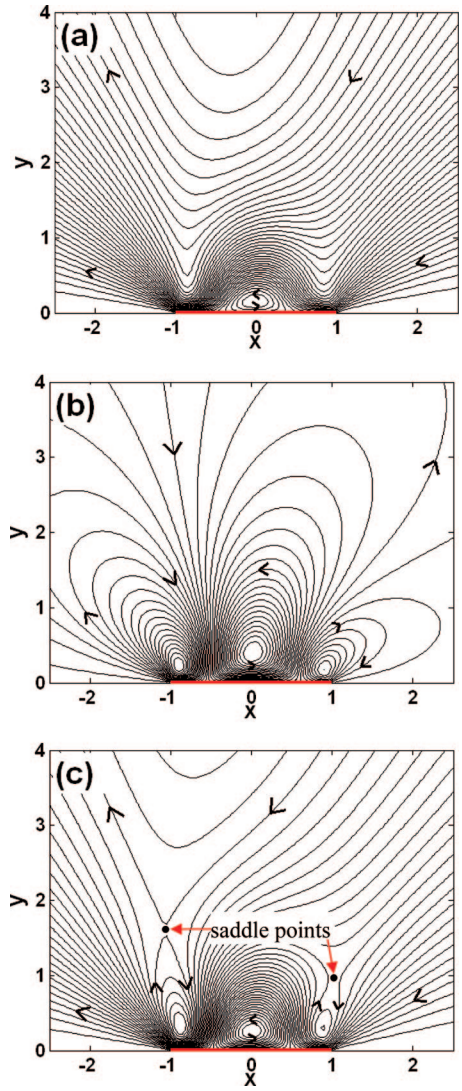

Figure 5. Illustration of flow patterns for EOF on a uniformly charged strip when applied electric fields are nonuniform: (a) $E_x = x^3 - 3x^2 - 0.25x + 0.5$, (b) $E_x = x^3 - 3x^2 - 0.25x + 1$, and (c) $E_x = x^3 - 3x^2 - 0.25x + 0.75$. The flow can exhibit various structures such as (a) closed eddy, (b) multiple vortices, and (c) saddle-point flow.

potential) and the local electric field on the basis of eq 1, it is straightforward to extend the analysis to systems in nonuniform fields. Because an applied field must be divergence-free and can generally be written in a simple harmonic form, the corresponding tangential field $E_{||}$ on the surface also behaves like x^m, whereas the associated normal field vanishes. Using the surface charge distribution of x^q, the resulting surface velocity becomes $f(x) = x^{m+q}$, and hence the solutions derived earlier are still applicable.

Recall in Figure 3 that symmetric and antisymmetric surface charge distributions lead to draining/pumping and vortex flow structures, respectively. An application of a nonuniform field can change the flow structure from one to another, depending on whether the field is in phase or out of phase with the surface charge distribution. For in-phase case, $f(x)$ will be symmetric and hence will lead to a simple in-and-out flow; on the contrary, out-of-phase case must develop a pair of vortices in response to an antisymmetric distribution of $f(x)$. In the case in which the applied field has a certain phase difference with the surface charge distribution, the flow will possess features of both symmetric and antisymmetric cases and hence will exhibit a variety of stream patterns such as closed eddy, multiple vortices, and saddle-point flow, as illustrated in Figure 5.

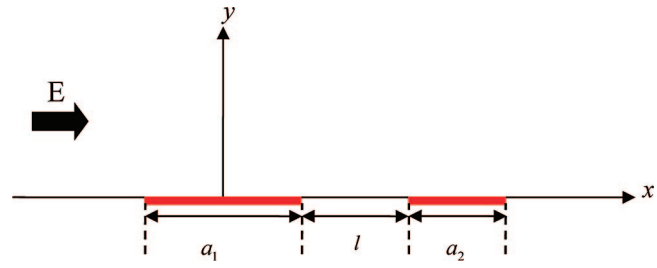

Figure 6. EOF set up by two charged strips in a uniform applied field.

III. Electro-osmotic Flow on Two Charged Strips

Motivated by the fact that a practical microdevice often comprises a number of patterned surfaces or arrays of microelectrodes, in this section we study EOF involving more than one charged strip. Hereafter we focus on a system with a pair of uniformly charged strips (Figure 6). Because the problem is linear, the solution can be constructed by a superposition of those for single-strip problems derived in the preceding section. Because the flow generated by one strip can interact with the other, the detailed flow structure will depend on the strips' charges (reflected by zeta potentials ζ_1 and ζ_2), widths (a_1 and a_2), and separation (l), which are characterized by the following parameters normalized by the quantities of strip 1:

$$\alpha = \zeta_2/\zeta_1, \beta = a_2/a_1, \gamma = l/a_1$$

To facilitate the subsequent discussion, we use $\zeta_1 < 0$ so that the slip velocity on strip 1 is always in the direction of the applied field. Combining two single-strip solutions from eq 13, we obtain the following stream function for EOF on two charged strips

$$\psi = \frac{y}{\pi}[\varphi_1 + \alpha\varphi_2] \text{with}$$
$$\varphi_1 = \tan^{-1}\left(\frac{y}{x^2 + y^2 - 0.25}\right),$$
$$\varphi_2 = \tan^{-1}\left(\frac{\beta y}{(x-d)^2 + y^2 - 0.25\beta^2}\right),$$
$$d = \gamma + (1+\beta)/2 \qquad (17)$$

Similarly, the corresponding velocity field reads

$$u = \frac{1}{\pi}[\varphi_1 + \alpha\varphi_2] + \frac{y}{\pi}[u_3 + \alpha u_4] \qquad (18a)$$

$$v = \frac{y}{\pi}[v_3 + \alpha v_4] \qquad (18b)$$

where (u_3, v_3) and (u_4, v_4) are derived from the two single-strip solutions

$$u_3 = \frac{x^2 - y^2 - 0.25}{(x^2 + y^2 - 0.25)^2 + y^2},$$
$$v_3 = \frac{2xy}{(x^2 + y^2 - 0.25)^2 + y^2},$$
$$u_4 = \frac{\beta((x-d)^2 - y^2 - 0.25\beta^2)}{((x-d)^2 + y^2 - 0.25\beta^2)^2 + \beta^2 y^2},$$
$$v_4 = \frac{2\beta(x-d)y}{((x-d)^2 + y^2 - 0.25\beta^2)^2 + \beta^2 y^2}$$

With the flow solution above, we now examine how the flow structure varies with the relevant parameters.

III.A. Effects of Strip Charges, Widths, and Separation on EOF Structure. Figure 7 shows how the charges of the equal-sized strips affect the EOF structure. Figure 7a,b shows the stream

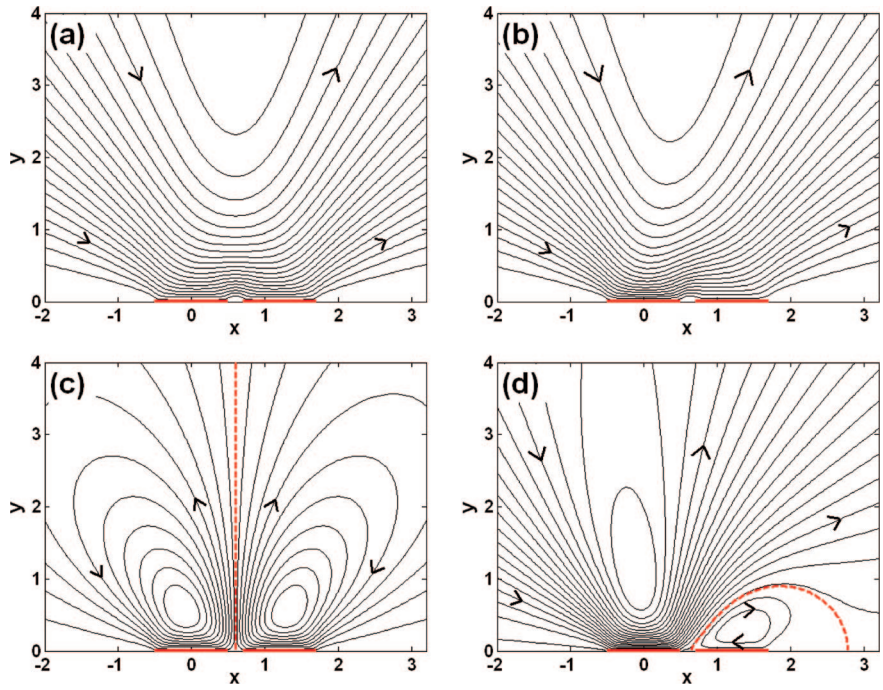

Figure 7. Effects of surface charge ratio α on the EOF pattern on two strips with (β, γ) = (1, 0.2). (a) α = 1, (b) α = 0.5, (c) α = −1, and (d) α = −0.3. In c and d, red dashed lines are either the streamline that separates the two vortices or the bounded streamline that encloses the confined eddy.

patterns when the strips bear like charge (α > 0). At first glance, the two concurrent surface flows yield simple draining-in and pumping-out stream patterns, similar to those in Figure 3a,c in the single-strip case. It is obvious that the result (Figure 7a) for the equal charge case α = 1 must be symmetric with respect to the midplane because of the reversibility of Stokes flow. For unequally charged strips, the flow structure becomes asymmetric (Figure 7b) with a slight shift toward the strip with more charges (left) because more streams tend to be drawn by the faster surface velocity.

Figure 7c,d shows the results for unlike-charge case α < 0. Because the two surface velocities now oppose each other, the flow must form vortices. If the charges are equal (α = −1), then Figure 7c shows a symmetric pair of microvortices with a zero net flow rate that resembles Figure 3b,d for single-strip case with antisymmetric charge distributions. Unequal opposite surface charges will generate a net EOF because of excess surface charge. Because this net flow is dictated by the vortex on the strip with more charges and tends to suppress that on the other, the vortex on the strip with less charges will be confined on the surface, creating the closed recirculating eddy shown in Figure 7d.

Figure 8 depicts the effects of strip size on the flow structure. Here we look at unlike-charge case with α = −1 and examine how the flow structure changes as a result of the interactions of the vortices. Again, if the strips are of equal dimensions, then the flow exhibits a symmetric vortex pair, as already shown in Figure 7c. When the size of one strip decreases, however, the associated vortex shrinks and is suppressed by the adjacent expanding vortex on the other, as depicted in Figure 8a−c. The explanation is that the situation here gradually approaches the single-strip limit $\beta \to 0$ in which the vortex on the larger strip will become so large that none of the streams leaving the strip will return.

Finally, we examine the effects of strip separation. We are again interested in unlike-charge case, and the results are shown in Figure 9. At large separations, the interactions between two vortices are so weak that the local flow behavior near each strip resembles that over a uniformly charged strip (cf. Figure 9b,d). At small separations, the two strips essentially act like a single strip having a step change in the zeta potential. Because the interactions between the vortices now are strong, the small vortex is suppressed by the larger one, giving rise to a closed eddy for the former (cf. Figure 9a,c).

III.B. Pumping Flow Rate. As demonstrated above, when the strips have like charges, the flow simply shows additive pumping via concurrent surface flows. If they bear uneven opposite charges, then the flow can exhibit a free stream accompanied by asymmetric vortices. The flow rate (per unit length) is

$$Q = \int_0^\infty u \, dy = \psi(\infty) - \psi(0) = \frac{1 + \alpha\beta}{\pi} \qquad (19)$$

which is determined solely by the zeta potentials and dimensions of the strips. Written in the dimensional form, this flow rate reads $Q^* = -\varepsilon(\zeta_1 a_1 + \zeta_2 a_2)E/(\pi\eta)$ in which $\zeta_1 a_1 + \zeta_2 a_2$ reflects the total number of surface charges through $\zeta_i \approx -\lambda\sigma_{si}/\varepsilon$, where λ is the double-layer thickness and σ_{si} is the surface charge density of the strip i. It is also evident that Q is independent of the strip separation γ.

As indicated by eq 19, for $1 + \alpha\beta > 0$ (< 0), strip 1 is more (less) charged than strip 2, and hence there is forward (backward) pumping with a flow rate of $Q^* > 0$ (< 0) with respect to the direction of the applied field. Compared to the single-strip case, it is obvious that the flow rate will be increased by the addition of the second like-charge strip. If the two strips are oppositely charged (α < 0), then the net flow rate is controlled by the strip with more charges. Because the vortices must be asymmetric in this case, a closed eddy must develop on the strip with less charges to match the flow direction of the free stream generated by the excess surface charge. At $1 + \alpha\beta = 0$, there will be no net flow at all because the surface charge of one strip is offset exactly by the opposite charge of the other. In this case, if the strips are of different sizes ($\beta = -1/\alpha$), then the two vortices will be separated by a nearly vertical streamline, as shown in Figure 10.

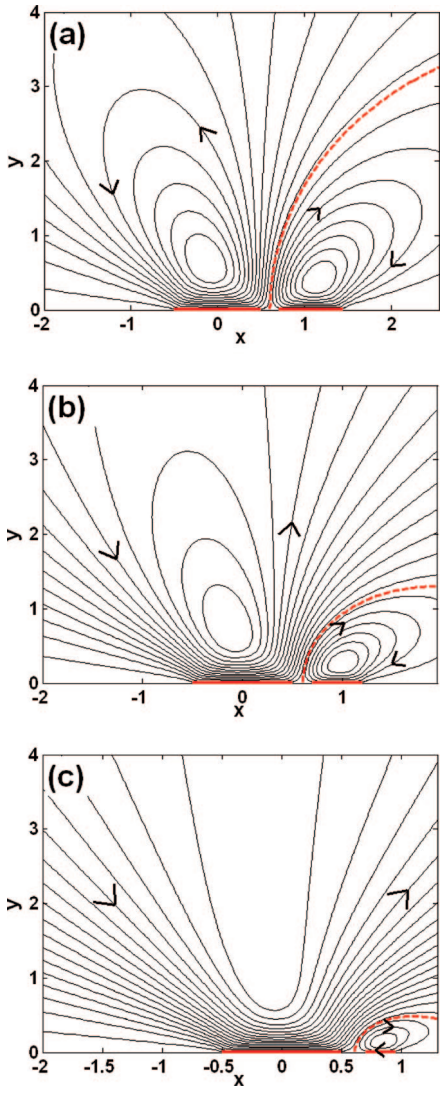

Figure 8. Effects of strip dimension ratio β on the EOF pattern on two oppositely charged strips with (α, γ)= (−1, 0.2): (a) $\beta = 0.75$, (b) $\beta = 0.5$, and (c) $\beta = 0.25$. Red dashed lines are the bounded streamlines that enclose the confined eddies.

Figure 11 summarizes how different flow topologies depend on α and β. The line $\alpha = 0$ defines the boundary between straight pumping of like-charge EOFs ($\alpha > 0$) and the occurrence of unlike-charge EOF vortices ($\alpha < 0$). Strip size ratio β does not alter the flow structure of the former but does change that of the latter because it controls the formation of vortices as well as flow reversal.

III.C. Formation of a Confined Eddy on Two Oppositely Charged Strips. As shown in the preceding sections, for two oppositely charged strips the flow can exhibit a closed recirculating eddy whose formation depends on the surface charge and strip dimensions. In particular, we are interested in the formation of such a confined eddy because it could play a vital role in transport processes involving samples with small diffusion coefficients. Because this eddy occurs within the confined streamline with two stagnation points, its size can be measured by the distance between these points. To determine the locations of the stagnation points, we set the stream function in eq 17 equal to zero and seek the interception of the bounded streamline to the surface. Mathematically speaking, these stagnation points, which exist only for $\alpha < 0$, are exactly the interception points of the associated ideal flow that is part of the solution structure as shown in section II.B. We also find that the locations of these points can be analytically determined only if α is a negative rational number. In practice, this analytical approach is sufficient because any arbitrary α can be approximated by a rational number. As such, we arrive at the following quadratic equation whose roots determine the locations of the stagnation points:

$$\frac{1}{4} - x^2 = -\alpha^{-1}\beta^{-1}\left[\frac{\beta^2}{4} - (x-d)^2\right] \tag{20}$$

The left- and right-hand sides in eq 20 come from φ_1 and φ_2 in eq 17, respectively. The stagnation points are thus located at

$$x_\pm = \frac{2d \pm \sqrt{4d^2 - (\alpha\beta+1)(4d^2 - \beta^2 - \alpha\beta)}}{2(\alpha\beta+1)} \tag{21}$$

where x_+ and x_- denote the respective locations of the two stagnation points. The distance L between these points then determines the size of the eddy and is given by

$$L \equiv x_+ - x_- = \frac{\sqrt{4d^2 - (\alpha\beta+1)(4d^2 - \beta^2 - \alpha\beta)}}{\alpha\beta+1} \tag{22}$$

Note that both eqs 21 and 22 are applicable only for $\alpha\beta < 0$ and $\alpha\beta + 1 \neq 0$ because the formation of a closed eddy can be realized only by two oppositely charged surfaces with nonzero net charge, as already discussed in section III.B. These conditions for α and β also ensure the validity of this analysis (via keeping the expression inside the square root in L always positive). In addition, $L > 0$ (<0) means that the eddy is located on the right (left), corresponding to $\alpha\beta + 1 > 0$ (< 0), viz., forward (backward) pumping with strip 1 having more (fewer) charges. To seek a better understanding of how the formation of a closed eddy depends on the strip charge and dimensions, below we restrict our attention to both small and large separation limits and discuss the results that follow.

In the $\gamma \to 0$ limit, the separation between the two strips is negligible compared to their dimensions (i.e., $\gamma \ll \min(1, \beta)$). The resulting stagnation points can be simplified as $x_+ = -1/2 + (1+\beta)/(1+\alpha\beta)$ and $x_- = 1/2$, and the latter is simply the right edge of strip 1, which is the junction between the two strips. The corresponding eddy size is therefore

$$L(\gamma \to 0) = \beta(1-\alpha)/(\alpha\beta+1) \tag{23}$$

Recall here that $\alpha < 0$. If the number of charges on strip 1 is greater than the number on strip 2 (i.e., $\alpha\beta + 1 > 0$), then a closed eddy must form over strip 2 because of flow suppression by the larger vortex on strip 1, which is in accordance with $x_+ > 1/2$ found here. In this case, eddy size L will grow monotonically with β because flow suppression is diminished by increasing the number of surface charges on strip 2. Further increasing β beyond $1/|\alpha|$ will lead to flow reversal in which the vortex on strip 2 can grow so large as to turn the confined eddy over onto strip 1 (viz., $L < 0$). For large β, we find that $L \approx 1/\alpha - 1$ and hence the confined eddy formed on strip 1 will be larger than the strip. Because the eddy size is now independent of the strip dimensions, it is determined solely by $(\zeta_1/\zeta_2) - 1$, the relative difference between the two surface zeta potentials: the smaller the difference, the larger the eddy size. Large β might be relevant to the scenario where there is a defect, for example, as a result of undesired deposition or incomplete etching, on the edge of a long strip. In that case, because a confined eddy can be triggered by minuscule variations in surface charge and transporting solutes across the eddy can be achieved only by diffusion, its appearance could be critical to mass transport processes. If α is allowed to be increased while keeping β fixed, we find that $L \approx -1$ for large α, which

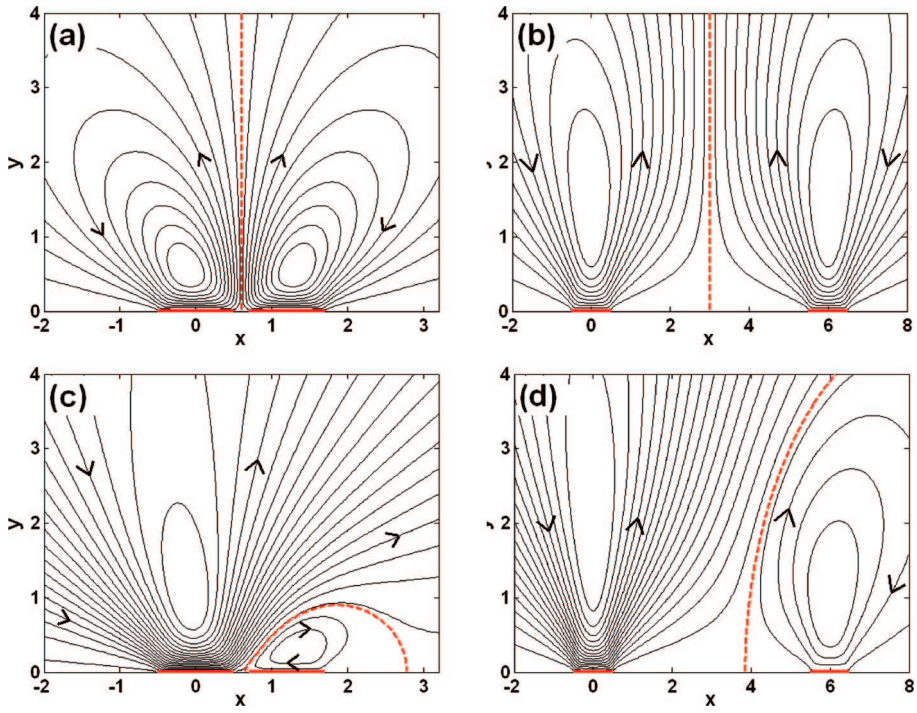

Figure 9. Effects of strip separation on the EOF pattern on two oppositely charged strips: (α, β, γ)= (a) (−1, 1, 0.2), (b) (−1, 1, 5), (c) (−0.3, 1, 0.2), and (d) (−0.3, 1, 5). Red dashed lines are either the streamlines that separate the two vortices or the bounded streamlines that enclose the confined eddies.

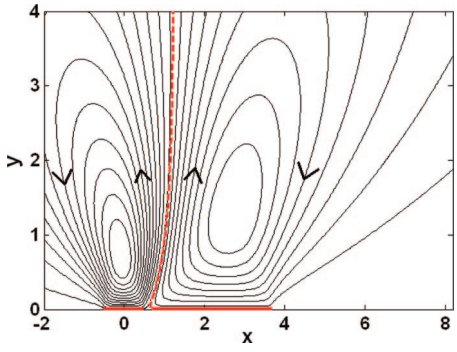

Figure 10. EOF streamlines when two oppositely charged strips are unequal in size but carry an identical number of charges: $\alpha = -1/3$, $\beta = 3$, and $\gamma = 0.2$. Two vortices now are separated by a nearly vertical streamline (red dashed line) in between.

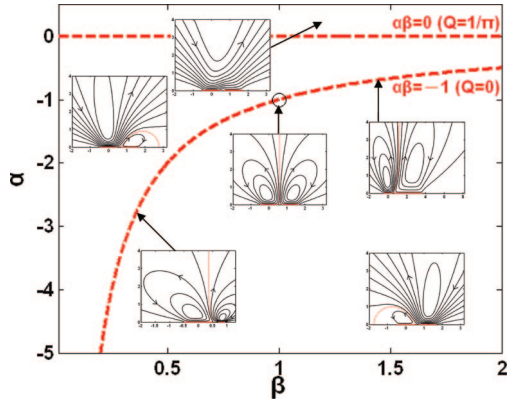

Figure 11. EOF map in the $\beta-\alpha$ plane for two uniformly charged strips in a uniform applied field. Various flow topologies can also be distinguished by the range of flow rate Q.

causes the eddy to be the same size as strip 1. The above results suggest that the eddy size is better controlled by the surface zeta potential difference, but the difference here cannot be too great if the eddy size is allowed to be adjustable.

As for the large separation limit, we find

$$L(\gamma \to \infty) = \left(\frac{-2\alpha\beta}{\alpha\beta + 1}\right)\gamma \tag{24}$$

suggesting that the eddy size grows linearly with the strip separation. In addition, the eddy size and its turning direction are further mediated by $\alpha\beta$, the ratio of the total surface charge on strip 2 to that on strip 1. For $|\alpha\beta| \ll 1$, eddy size $L \approx -\alpha\beta\gamma$ is controlled by strip 2. However, if $|\alpha\beta| \gg 1$, then we have $L \approx -2\gamma$, yielding the eddy of twice the size of the strip separation.

IV. Particle Trapping Assisted by EOF Vortices

In practical microfluidic applications, nonuniformly charged EOF can be used to facilitate the assembly of colloidal particles,[11,29] assist in concentrating pathogens for increasing detection susceptibility,[30] or enhance heterogeneous assays.[31] The idea behind such a manipulation is that EOF vortices can work with near-surface effects such as electrostatic attraction or dielectrophoresis to promote the trapping of particles on the surface by rapidly bringing suspended particles down onto the surface. Alternatively, from a kinetic point of view, transport processes driven by common colloidal forces or short-range effects are often limited by diffusion or lack the ability to capture particles distantly and hence are less efficient at trapping or concentrating suspended particles. The use of EOF vortices can facilitate short-range particle trapping by overcoming such a deficiency in such a way that particle are first brought onto the strips by the vortices with a converging stagnation point and then focused by the surface

(29) Islam, N.; Lian, M.; Wu, J. *Microfluid. Nanofluid.* **2007**, *3*, 369–375.
(30) Gagnon, Z.; Chang, H. C. *Electrophoresis* **2005**, *26*, 3725–3737.
(31) Feldman, H. C.; Sigurdson, M.; Meinhart, C. D. *Lab Chip* **2007**, *7*, 1553–1559.

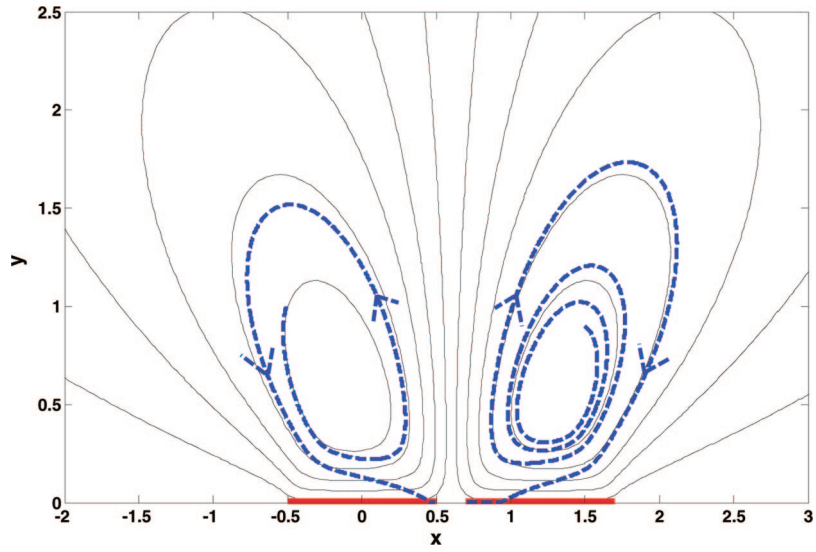

Figure 12. Particle trajectories (in blue dashed lines) in a pair of symmetric EOF vortices (in black lines) with a converging stagnation point in the middle of the surface: $\alpha = -1$, $\beta = 1$, $\gamma = 0.2$, $\upsilon_0 = 0.45$, and $\delta = 0.1$.

streams toward that point. And yet, we have to emphasize that the vortices alone do *not* trap particles because the flow is divergence-free and particles can still be dispersed away by the upward flow after focusing at the stagnation point—short-range attraction effects must be incorporated for realizing the trapping by holding particles against the upward flow near the stagnation point.

In this section, we employ the EOF solution developed in the preceding sections to illustrate numerically the use of EOF vortices in particle trapping. While the actual phenomenon has been reported previously using ac fields,[30,32] our dc-based ansatz complements these studies in the sense that it provides a relatively simple approach for eliciting qualitative features of the phenomenon. To do so, we consider the motion of nondiffusive particles in EOF vortices set up by a pair of oppositely charged strips of equal width. For simplicity, hydrodynamic interactions between the particles and the surface are assumed to be negligible. Interparticle interactions are also neglected. The instant particle position $\mathbf{x}_p(t) \equiv (x_p(t), y_p(t))$ is then determined by the following (dimensionless) equation

$$\frac{d\mathbf{x}_p}{dt} = \mathbf{v} + \mathbf{v}_{trap} \tag{25}$$

with $\mathbf{v}$ being the flow field given by eq 18 and t the dimensionless time scaled by a/U_0. Here $\mathbf{v}_{trap} = -|\mathbf{v}_{trap}|\ \mathbf{i}_y$ is the additional velocity accounting for the short-range attraction by the strips and is applicable only near the strips, outside of which $\mathbf{v}_{trap} = 0$. This velocity is assumed to be of the following form

$$\mathbf{v}_{trap} = -\upsilon_0 \exp(-y/\delta)\mathbf{i}_y \tag{26}$$

where υ_0 (> 0) is the trapping susceptibility and is reflected by the velocity magnitude of the short-range effect relative to the characteristic Smoluchowski velocity U_0 and δ measures the range of the attraction force, beyond which the force decays very rapidly. Equation 26 can be used to describe the motion of a charged particle due to electrostatic attraction by an oppositely charged surface if the particle comes close to the surface within a certain distance of the electric double layer δ.[33] It can also model particle trapping by dielectrophoresis (DEP) due to local field gradients when a particle is in close proximity to an electrode.[34] In this case, δ represents the penetration depth of the electric field.

Equation 25 is integrated numerically using the explicit Euler method with a time step of 0.01. Throughout the simulations, we assume that the particle's normal velocity vanishes when it hits the strips but still allows the particle to move horizontally on the strips. Figure 12 depicts the simulated particle movement in a pair of symmetric EOF vortices with a converging stagnation point in the middle of the surface. Initially, a particle is placed at an arbitrary position above the left strip. The particle is then carried by the vortex in a counterclockwise manner. Because of $\mathbf{v}_{trap}$, there are small deviations from the streamlines in the particle trajectory, making the particle move spirally toward the surface. When it is close to the strip (i.e., within δ), it will perceive a more pronounced attraction force and hence in turn will be redirected toward the strip with an abrupt change in its motion. Upon attaching to the strip surface, the particle is then advected by the surface flow toward the stagnation point, at which the particle will eventually be at rest because of zero velocity. Because a similar phenomenon equally occurs on the right strip, the effect looks as if particles were brought down by the vortices and focused toward the middle of the surface.

If the flow (or field) direction is reversed, then the local flow field near the stagnation point now becomes diverging. In this case, our simulation (not shown) indicates that instead of being focused, particles are diverted away from the middle when coming down toward the surface. A closer further inspection reveals that particles will eventually be recycled back to the bulk. Consequently, there is no trapping at all on the strips. Near a diverging stagnation point, the flow is coming from the top toward the point and then turning away from it when impinging the surface. The closer to the surface, the faster a particle is diverted away by the flow, making the particle recirculate back to the bulk. These observations confirm the idea that the use of EOF vortices in particle trapping must be accomplished with a converging

(32) Wu, J.; Ben, Y.; Battigelli, D.; Chang, H. C. *Ind. Eng. Chem. Res.* **2005**, *44*, 2815–2822.

(33) Hunter, R. J. *Foundations of Colloid Science*, 2nd ed.; Oxford University Press: New York, 2001.

(34) For DEP in a nonuniform electric field created by, for instance, an array of interdigitated electrodes, it can be easily seen by solving the Laplace equation that the electric field decays exponentially in y and hence does the corresponding DEP velocity.

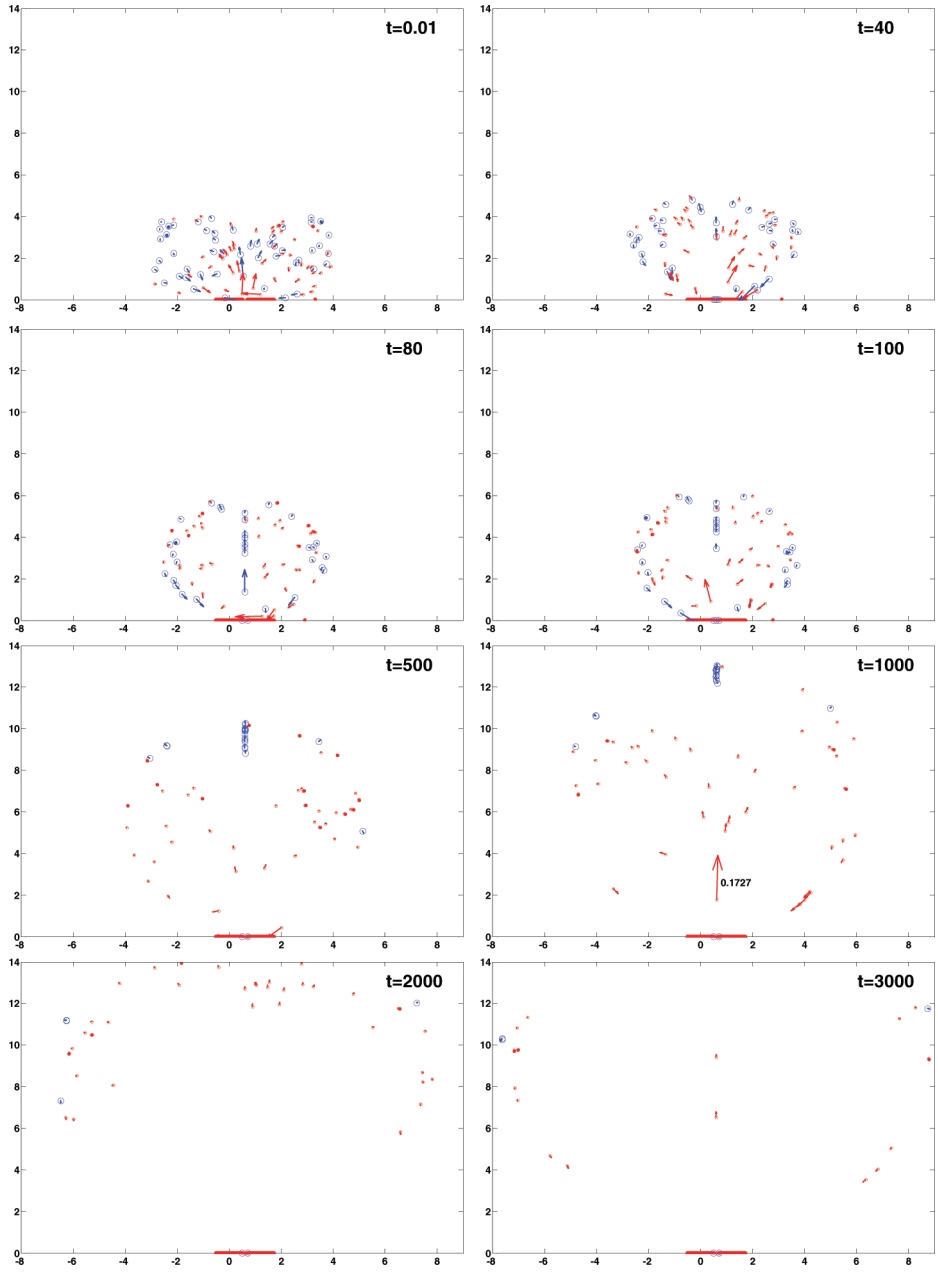

Figure 13. Evolution of a particle suspension consisting of two particle populations: $v_0 = 0.45$ (blue) and 0.045 (red) with 50 particles for each. Flow conditions are the same as in Figure 12. Arrows represent instant velocity vectors of these particles. The number in the $t = 1000$ panel is for a referenced velocity scale. Most of the blue particles are captured by the strips before $t \approx 500$, whereas only a small fraction of red particles have landed for $t > 1000$.

stagnation point, which can be simply controlled by the direction of an applied field.

To illuminate further such EOF-assisted particle trapping, we carry out simulations for a suspension consisting of two particle populations with different trapping susceptibilities (via v_0). As shown in Figure 13, the particles of the larger v_0 are quickly brought onto the strip surface, whereas those of the smaller v_0 tend to be recirculated in the bulk and take a longer time to land on the surface. To quantify the results observed above, Figure 14 plots the fraction of particles trapped on the strip surface as a function of time and clearly shows that the trapping is indeed more efficient for particles of larger v_0. Because v_0 can reflect part of the particle identity (e.g., size, charge, conductivity, etc.), the present results suggest that particle sorting can be achieved more efficiently with the assistance of EOF vortices, which is in accordance with experimental observations.[30] For a given particle population, however, decreasing v_0 can also indicate the increasing speed of the flow. This suggests that the ability to capture particles could be compromised if the vortices are too fast because particles are recirculated more rapidly in the bulk and thus less susceptible to being captured by the surface through the short-range attraction.

It is also interesting to see what happens to a suspension of particles if the vortices become asymmetric as a result of unequal numbers of opposite surface charges. This might simulate the scenario where there is anomalous adsorption or nonuniform particle deposition on the surface, which could modify the surface zeta potential and hence the flow structure. Because there are two stagnation points on the edges of the confined eddy and the corresponding local flow fields can be either converging or diverging, the trapping behavior obviously depends on the flow direction (and hence the direction of the applied field). Also,

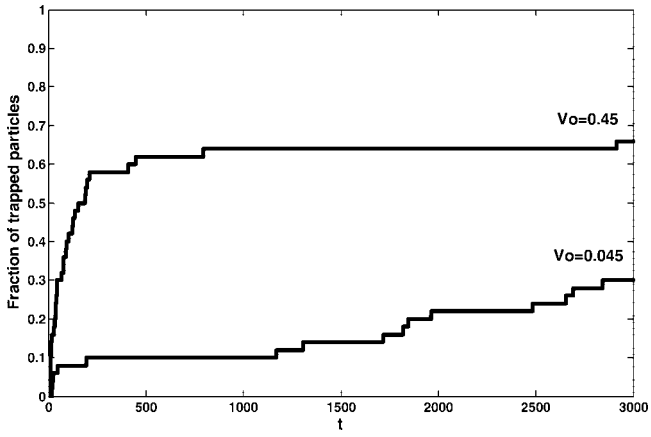

Figure 14. Comparison between the trapped-particle fractions for two particle populations with different trapping susceptibilities. Flow conditions are the same as in Figure 12.

because the flow structure now is asymmetric the ultimate fate of a particle seems to depend on where it is located and how it is influenced by the flow field during its journey.

Figure 15 shows the evolution of the motion of a particle suspension in which there is a net flow toward the right with a converging (diverging) stagnation point on the left (right) of the confined eddy. We find that the particles on the left are quickly brought onto the surface by the larger vortex and focused toward the left stagnation point by the converging surface flow, similar to the result in symmetric vortex case. As for the particles on the right, however, because of the presence of the confined eddy, the particles outside the eddy are depleted by the free stream whereas those inside can still be focused toward the left stagnation point. Note here that the right stagnation point of the confined eddy does not permit focusing because the local surface flow diverges away from that point. As such, there exists a depletion zone between the vortices in which it is unlikely that trapping occurs.

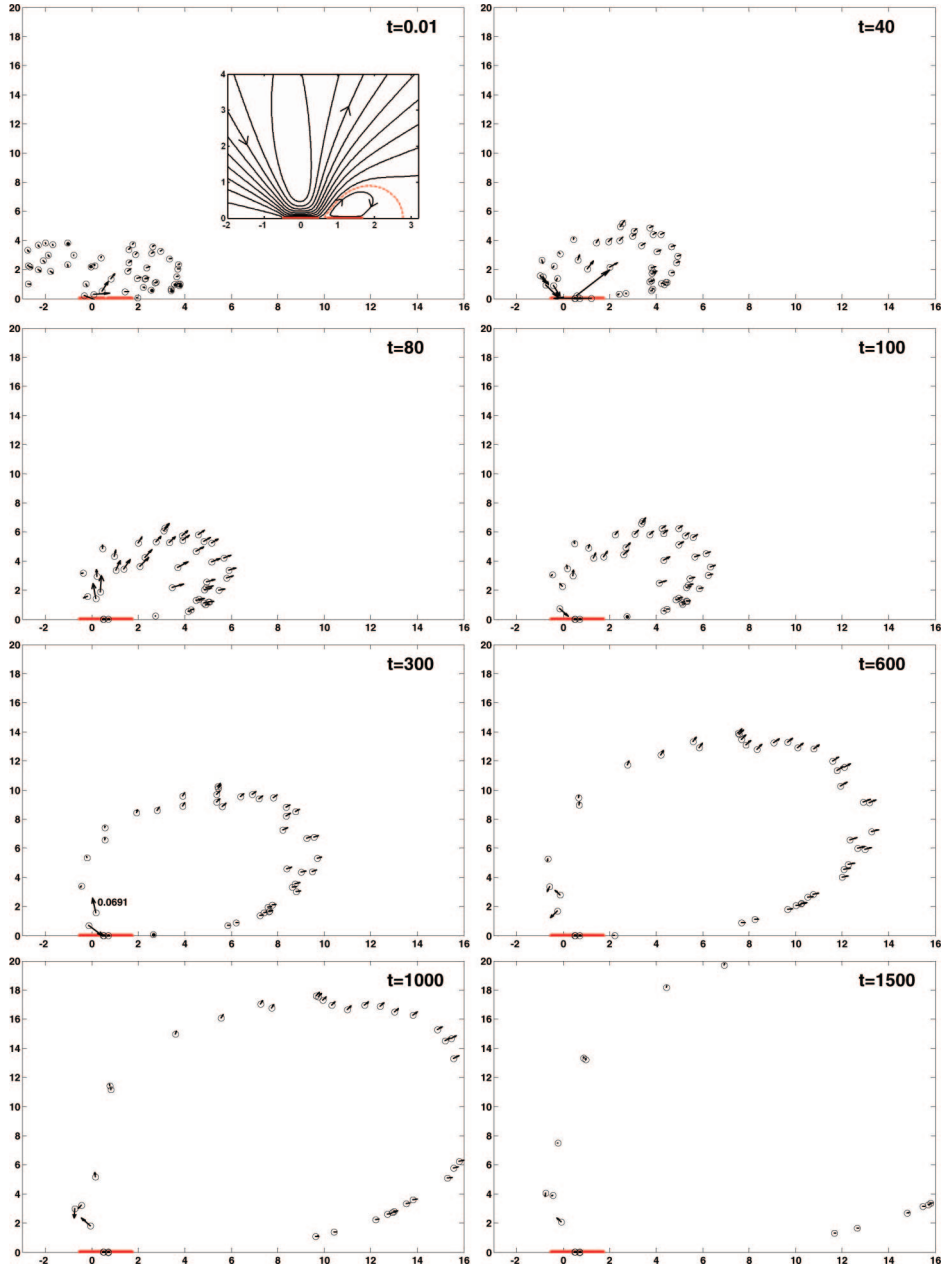

Figure 15. Evolution of particle motion in asymmetric EOF vortices with a stream pattern shown in the $t = 0.01$ panel. Fifty particles are used in this case: $\alpha = -0.3$, $\beta = 1$, $\gamma = 0.2$, $v_0 = 0.45$, $\delta = 0.1$. The number in the $t = 300$ panel is a referenced velocity scale.

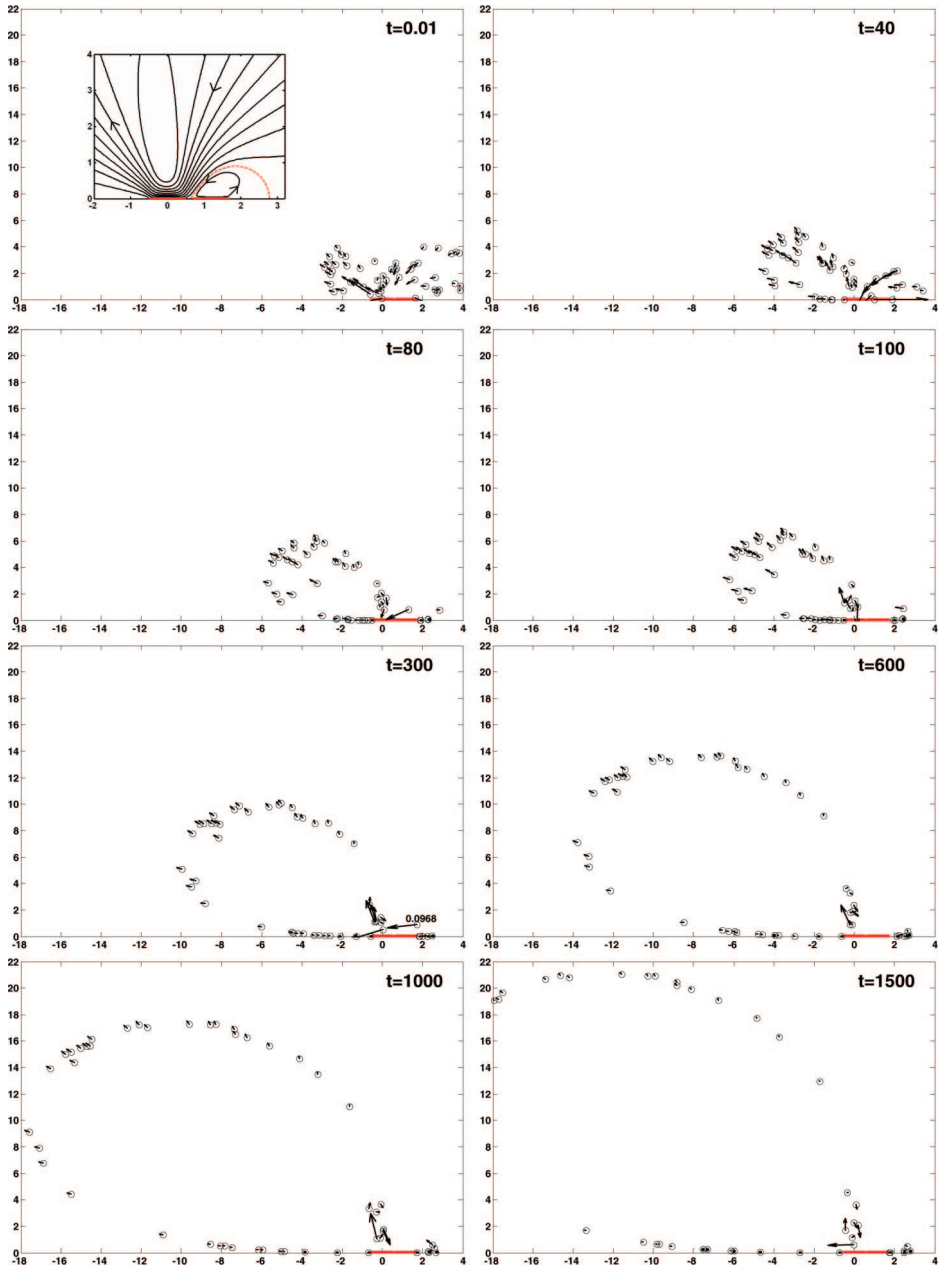

Figure 16. Evolution of the particle motion with the opposite applied field direction to that in Figure 15. The stream pattern is shown in the $t = 0.01$ panel. Fifty particles are used in this case.

Figure 16 is the result with the field direction opposite to that in Figure 15. We find that particles can no longer be focused at the left stagnation point around which the local surface flow becomes diverging. Because the converging stagnation point now is switched to the right, it seems that particles can be trapped only there. However, because most of the particles are gradually dispersed toward the left by the counterclockwise vortex, there are virtually no trapping effects in this case.

A comparison between the trapping efficiencies using symmetric and asymmetric vortices is shown in Figure 17, suggesting that it is more desirable to use *symmetric* vortices with *converging* stagnation in the trapping. Hence, we speculate that any nonuniformity in surface charge could be critical to actual trapping processes. For instance, if particles are charged and deposited unevenly on the surface, then the surface zeta potentials could be altered by these deposited particles, making the vortex structure asymmetric and thereby affecting subsequent particle motion behavior.

It is instructive to compare EOF-based particle trapping with trapping by DEP that is widely used in microfluidic systems and has been proven to be quite successful. In DEP trapping, the particle movement is caused by charge polarization of a particle under the action of a nonuniform electric field. The particle's DEP velocity is described by $v_{DEP} = (\varepsilon_m/3\eta)R^2K\nabla|E|^2$ with K being the effective polarizability and R being the particle size.[2] For most of the common colloids, because of the quadratic dependence on R, v_{DEP} is on the order of 10 μm/s under typical experimental conditions. This is much slower than an EOF velocity of about 100 μm/s under similar conditions. Also because sufficiently large field gradients are required to render apparent particle movement, trapping usually occurs in areas such as sharp electrode edges or within a short distance to a surface. Despite the small mobility and short-range characteristics, DEP trapping is rather selective in view of its dependence on particle/solvent properties (via K) and hence has advantages in sorting particles.

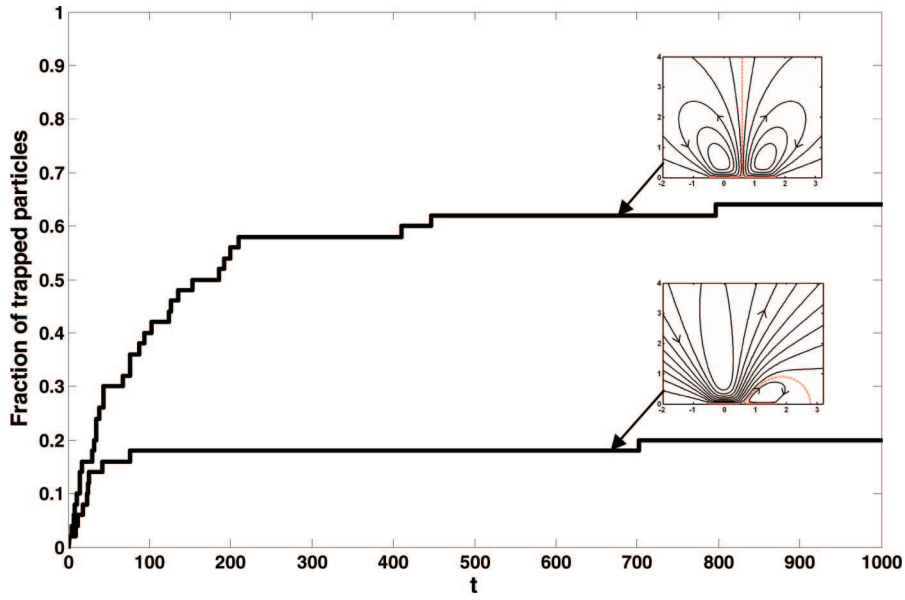

Figure 17. Comparison between trapped-particle fractions using symmetric and asymmetric EOF vortices. The former and the latter are the data from Figures 13 and 15, respectively. There is virtually no particle trapping in Figure 16.

In contrast to DEP trapping, EOF-based particle trapping is a collaborative phenomenon of long-range convective transport and short-range surface attraction effects. Although it has the ability to trap particles distantly at much faster rates than DEP, the efficiency will depend on the detailed flow structure and the nature of the short-range effects. In some cases, the trapping could be compromised if subjected to inadequate flow conditions (e.g., when the vortices are turned outward or are asymmetric). Also, because of advection by the flow, the trapping might not be as definite or selective as DEP.

V. Concluding Remarks

In this article, we have analyzed theoretically the detailed characteristics of EOF on charged strips. Our approach invokes the ideal-flow analogy that not only enables us to construct an analytical solution for the flow but also furnishes a lucid way to identify the flow behavior. For an EOF on a single charged strip, we find that the flow can exhibit a simple in-and-out streaming, a pair of symmetric vortices, and an asymmetric vortex structure, depending on the surface charge distribution. Our analysis can also be applicable to systems with nonuniform applied fields. In this case, the combined effects of surface charge and applied field can lead to more complicated flow structures involving multiple vortices or saddle points. An extension to EOF on two uniformly charged strips is also carried out, and the solution can be readily constructed by a superposition of the solutions to single-strip problems. We demonstrate how the flow structure varies with the strip surface charges and dimensions. A variety of flow topologies can also be identified analytically in line with how the flow rate and the formation of a confined eddy are mediated by these factors.

Our study also reveals that the fluid velocity here decays at a rate of $1/r$ or $1/r^2$. This long-range hydrodynamic nature suggests that the effects of proximate boundaries on fluid motion could be important, for instance, if there is a boundary above the surface with separation comparable to the strip size[10] or if the flow occurs in an open cavity[20] or closed box.[21] In addition, because the velocity now attenuates much more slowly than $1/r^3$ in electrophoretic interactions,[27] hydrodynamic interactions between suspended particles and the surface could become important, which could play a crucial role in the dispersion behavior of colloidal suspensions. Although real systems are always bounded, our analysis provides a more thorough understanding of the local flow behavior near the surface, and the results here might not be too qualitatively different from those in confined systems if proximate boundaries are not too close to the surface.

Finally, we demonstrate numerically the use of EOF in particle trapping. By including short-range attraction effects in the particle velocity, we show that the trapping can be expedited by symmetric EOF vortices in such a way that suspended particles are quickly brought by the vortices onto the surface, followed by hydrodynamic focusing toward the stagnation point. Our results also suggest that it is less desirable to use asymmetric vortices to trap particles because of depletion by free streams. Actual trapping processes could involve colloidal/hydrodynamic interactions between particles and surfaces, the dispersion/aggregation behavior of particles, and changes in surface zeta potentials due to particle deposition. Nevertheless, to the best of our knowledge, this is the first attempt of modeling the use of EOF in particle trapping and might provide some insights into trapping processes in practice.

In conclusion, the present study not only provides a systematic framework for analyzing EOF and its use in particle trapping but also offers useful guidance for the design of microfluidic devices.

Acknowledgment. This work was supported by the National Science Council of Taiwan under grants NSC 94-2214-E-006-023 to S.-H.H. and NSC 96-2221-E-006-055 to H.-H.W.

Appendix I: Far-Field Behaviors of the Two Ideal-Flow Solutions

As $r \to \infty$ the two ideal-flow solutions (eqs 11a and 11b) have the following asymptotic behaviors:

$$\chi_1^{\infty} = \frac{2\sin\theta}{\pi r} + O(r^{-2}),$$
$$u_1^{\infty} = \frac{2\cos(2\theta)}{\pi r^2} + O(r^{-3}),$$
$$v_1^{\infty} = \frac{2\sin(2\theta)}{\pi r^2} + O(r^{-3}) \qquad \text{(A1)}$$

$$\chi_2^{\infty} = \frac{2\cos\theta}{\pi r} + O(r^{-2}),$$
$$u_2^{\infty} = -\frac{2\sin(2\theta)}{\pi r^2} + O(r^{-3}),$$
$$v_2^{\infty} = \frac{2\cos(2\theta)}{\pi r^2} + O(r^{-3}) \quad \text{(A2)}$$

Appendix II: Far-Field Behavior of EOF on a Charged Strip

This appendix provides the corresponding $r \to \infty$ behaviors for the EOF solutions (eqs 13−16).

$$f = 1: \quad u = \frac{2\sin(2\theta)\cos\theta}{\pi r} + O(r^{-3}),$$
$$v = \frac{2\sin(2\theta)\sin\theta}{\pi r} + O(r^{-3}) \quad \text{(A3)}$$

$$f = x: \quad u = \frac{2\sin(4\theta)}{3\pi r^2} + O(r^{-4}),$$
$$v = \frac{4\sin(3\theta)\sin\theta}{3\pi r^2} + O(r^{-4}) \quad \text{(A4)}$$

$$f = x^2: \quad u = \frac{2\sin(2\theta)\cos\theta}{3\pi r} + O(r^{-3}),$$
$$v = \frac{2\sin(2\theta)\sin\theta}{3\pi r} + O(r^{-3}) \quad \text{(A5)}$$

$$f = x^3: \quad u = \frac{2\sin(4\theta)}{5\pi r^2} + O(r^{-4}),$$
$$v = \frac{4\sin(3\theta)\sin\theta}{5\pi r^2} + O(r^{-4}) \quad \text{(A6)}$$

Appendix III: EOF Solution with an Arbitrary Integer-Power Charge Distribution

For an arbitrary integer-power charge distribution $f = x^n$, we can also obtain a solution for the stream function which can be expressed in a complex-variable form below. Let $z = x + iy$. For symmetric charge distributions of $n = 2N$ ($N = 0, 1, 2,...$),

$$\psi = y\left[(-1)^{2N} Re((-iz)^{2N})\chi_1 + (-1)^{2N-1} Im((-iz)^{2N})\chi_2 + \frac{2}{\pi}\sum_{p=1}^{N} \frac{(-1)^{p-1}}{2(N-p)+1} Re((-iz)^{2p-1})\right] \quad \text{(A7)}$$

For antisymmetric charge distributions of $n = 2M - 1$ ($M = 1,2,3,...$),

$$\psi = y\left[(-1)^{M} Im((-iz)^{2M-1})\chi_1 + (-1)^{M} Re((-iz)^{2M-1})\chi_2 + \frac{2}{\pi}\sum_{q=1}^{M} \frac{(-1)^{q-1}}{2(M-q)+1} Im((-iz)^{2q-2})\right] \quad \text{(A8)}$$

where χ_1 and χ_2 are defined in eq 11.

LA802183Q